

Two-dimensional Inside-out Eaton Lens: Wave Properties and Design

Yong Zeng and Douglas H. Werner

Department of Electrical Engineering, Pennsylvania State University, University Park, PA 16802

In this paper we study two-dimensional inside-out Eaton lens theoretically and numerically. With the help of the WKB approximation, we investigate the finite-wavelength effect analytically and demonstrate one necessary condition for perfect imaging by the lens. Furthermore, we present one example design and test its performance by using full wave Maxwell solvers.

More than half a century ago, it was proposed that gradient index lenses [1], such as the Maxwell fish-eye lens [2], the Luneburg lens [3] and the Eaton lens [4], can be free of geometrical aberrations and form perfect images, at least at the geometrical-optics level (see Reference [5] and [6] for more details). Taking the inside-out Eaton lens as an example, its refractive index $n(r)$ equals $\sqrt{(2-r)/r}$ for $1 \leq r \leq 2$ and 1 otherwise, with r being the radius (see Figure 1). We can analytically prove that light rays emitted from a source at position \mathbf{r}_0 , with $r_0 < 1$, will be focused exactly at position $-\mathbf{r}_0$ [6]. Therefore, like Maxwell's fish-eye lens, perfect imaging can be obtained by an inside-out Eaton lens, and both the source and the image are inside the optical instruments.

Recently, a renaissance of scientific interests appears in these gradient index lenses [7–12], partially because of the developments of metamaterials [13, 14] and transformation optics [15–18]. Metamaterials are manmade media whose effective permittivities and permeabilities are determined by their deeply subwavelength structures as well as their constituent materials [14]. For instance, integrating split ring resonators with metallic rods will result in a metamaterial with an effectively negative index of refraction [19]. Transformation optics, on the other hand, is inspired by an intriguing property of Maxwell's equations, *i.e.*, their form is invariant under arbitrary coordinate transformations, assuming the field quantities and the material properties are transformed accordingly [15, 16].

In this paper, we design a two-dimensional dielectric inside-out Eaton lens consisting of metallic wires in a homogeneous background medium with positive permittivity. To investigate the effect of the finite wavelength, we employ the WKB approach to solve the wave equations [20, 21], and obtain one necessary condition for perfect imaging. Finally we test our design with full wave Maxwell solvers.

The original Eaton lens has a spherical geometry and an index of refraction as

$$n(r) = \sqrt{\frac{2}{r} - 1}, \quad (1)$$

with r being the radius [4]. Since it possesses spherical symmetry, the entire ray trajectory lies in a plane which is orthogonal to a conserved angular momentum \mathbf{L} [6] (See Appendix A). Consequently, we can simplify it to be a two-dimensional cylinder with similar refractive index. We further assume that the cylinder lies in the xy plane, as well as the propagation plane of the light ray. Moreover, we only consider TM-polarized light where the magnetic-field vector \mathbf{H} points in the z direction. By sacrificing the impedance matching, we can further assume that the two-dimensional cylinder is purely electrical, *i.e.* $\mu = 1$, with its permittivity $\epsilon(r)$ given by $n^2(r)$.

A detailed ray-optics description of the inside-out Eaton lens can be found in Ref. [6], and it is repeated in Appendix

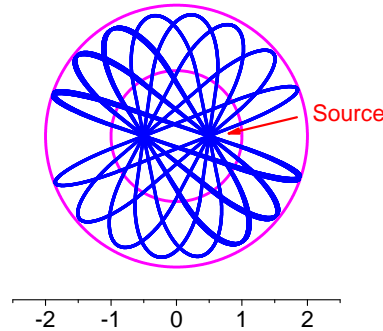


FIG. 1: Inside-out Eaton Lens ($1 \leq r \leq 2$). The source is located at $r_0 = 0.5$. Light rays (blue) are described by Hamilton's equation (A.2).

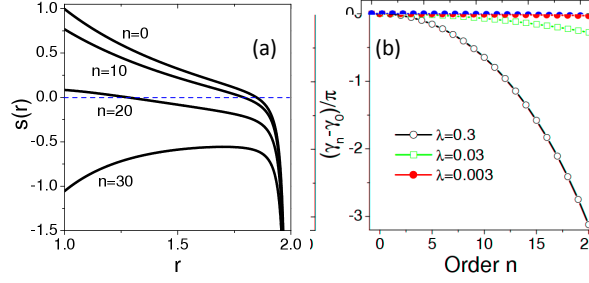


FIG. 2: (a) Dependence of the function $s(r)$ on the mode order n . Here the wavelength is 0.3. (b) Effect of the wavelength λ on the phase factor γ_n .

A for the convenience of readers. We therefore only consider the wave interpretation here. Starting from the following wave equation

$$\frac{1}{\epsilon(r)} \nabla^2 H + \nabla \frac{1}{\epsilon(r)} \cdot \nabla H = -\frac{\omega^2}{c^2} H, \quad (2)$$

with $\nabla = \partial_x \mathbf{e}_x + \partial_y \mathbf{e}_y$ and H as H_z , this equation can be reformulated in cylindrical coordinates as

$$\frac{\partial^2 H}{\partial r^2} + \left(\frac{1}{r} - \frac{1}{\epsilon} \frac{d\epsilon}{dr} \right) \frac{\partial H}{\partial r} + \frac{1}{r^2} \frac{\partial^2 H}{\partial \theta^2} + k_0^2 \epsilon H = 0, \quad (3)$$

with $k_0 = \omega/c$ being the wave number in free space. We now assume that the magnetic field $H(r, \theta)$ can be expanded as $\sum_n f_n(r) e^{in\theta} \sqrt{\epsilon/r}$, where the functions f_n satisfy

$$f_n'' + \left(k_0^2 \epsilon - \frac{n^2}{r^2} + \frac{\epsilon^2 - 3r^2 \epsilon'^2 + 2r\epsilon\epsilon' + 2r^2 \epsilon\epsilon''}{4r^2 \epsilon^2} \right) f_n = 0. \quad (4)$$

In the region $r \leq 1$ where $\epsilon(r) = 1$, we have

$$f_n'' + \left(k_0^2 - \frac{n^2 - 1/4}{r^2} \right) f_n = 0, \quad (5)$$

and express the solutions generally as

$$f_n(r) = \sqrt{r} \left[a_n H_n^{(1)}(k_0 r) + b_n H_n^{(2)}(k_0 r) \right], \quad (6)$$

where $H_n^{(1)}$ and $H_n^{(2)}$ are the n -th order Hankel functions of the first and second kind, respectively. In the region $1 < r < 2$, we can rewrite Equation (4) as

$$f_n'' + s(r) k_0^2 f_n = 0, \quad (7)$$

with

$$s(r) = \frac{2-r}{r} - \frac{n^2 - 1/4}{r^2 k_0^2} - \frac{r+1}{r^2 (2-r)^2 k_0^2}. \quad (8)$$

A few examples are plotted in Figure (2). For a modest n , $s(r)$ generally monotonically decreases from a positive value to negative infinity. It is however always negative when n is large enough.

We employ the WKB approximation, developed by Wentzel, Kramers and Brillouin in 1926, to analytically solve Equation (7) with a modest n [20, 21]. More specifically, we assume that $f_n(r)$ has the form $A_n e^{ik_0 \tau(r)}$ for positive $s(r)$, and $\tau(r)$ can be further expanded in terms of k_0 ,

$$\tau(r) = \tau_0(r) + \frac{1}{k_0} \tau_1(r) + \frac{1}{k_0^2} \tau_2(r) + \dots. \quad (9)$$

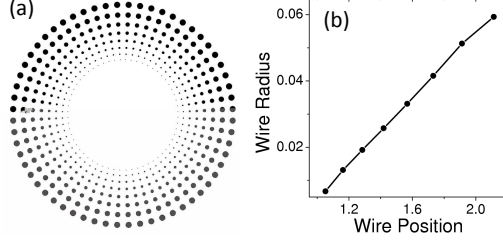


FIG. 3: (a) A schematic of the design. (b) The radius of the metallic wire as a function of its position. Here the permittivity of the metal is $\epsilon_m = -0.6$.

Similar arguments also hold by $\tau'(r)$ as well as $\tau''(r)$. By collecting the leading-order terms, it is found that

$$\left(\frac{d\tau_0}{dr}\right)^2 = s(r), \quad \frac{d\tau_1}{dr} = \frac{i\tau_0''}{2\tau_0'}. \quad (10)$$

Consequently the first order solution can be expressed as

$$f_n(r) \sim \frac{A_n^+}{s(r)^{1/4}} \exp\left[ik_0 \int_{r_n}^r \sqrt{s(r')} dr'\right] + \frac{A_n^-}{s(r)^{1/4}} \exp\left[-ik_0 \int_{r_n}^r \sqrt{s(r')} dr'\right], \quad (11)$$

with r_n standing for the turning point where $s(r) = 0$. The first term on the right hand side corresponds to an out-going wave because its phase increases with distance, while the second term corresponds to an in-coming wave. Similar procedures can be applied to a negative $s(r)$ by assuming $f_n(r) = B_n e^{-k_0 \tau(r)}$, and the resultant first-order approximation is given by

$$f_n(r) \sim \frac{B_n^+}{|s(r)|^{1/4}} \exp\left[-k_0 \int_{r_n}^r \sqrt{|s(r')|} dr'\right]. \quad (12)$$

Here only the solution that is exponentially decaying in the r direction is included. Furthermore, $s(r) \sim (r_n - r)$ approaches zero linearly in the vicinity of the turning point r_n . The solution therefore can be approximated as $\text{Ai}(-k_0^{2/3} s)$, with Ai being the Airy function [20]. When k_0 is large enough, we can asymptotically match Equation (11) and (12) around the turning point, and finally achieve $A_n^+ = iA_n^-$. As a direct result, in the region where $s(r)$ is positive, we have

$$f_n(r) \sim \frac{A_n}{s(r)^{1/4}} \exp\left[ik_0 \int_{r_n}^r \sqrt{s(r')} dr'\right] + \frac{A_n}{s(r)^{1/4}} \exp\left[-i\frac{\pi}{2} - ik_0 \int_{r_n}^r \sqrt{s(r')} dr'\right], \quad (13)$$

which implies that an out-going wave will be totally reflected around the turning point r_n , accompanied with a phase variation of $\pi/2$.

We now assume Equation (13) can be extended to the region where r is slightly smaller than 1. Additionally, its phase factor can be approximated as

$$k_0 \int_{r_n}^r \sqrt{s(r')} dr' = k_0 \int_{r_n}^r \sqrt{s_0} dr' + k_0 \int_{r_n}^1 \left[\sqrt{s(r')} - \sqrt{s_0}\right] dr' \approx k_0 r + \gamma_n, \quad (14)$$

where γ_n does not depend on r , and

$$k_0^2 s_0 = k_0^2 - \frac{n^2 - 1/4}{r^2} \quad (15)$$

being the coefficient shown in Equation (5). In the vicinity of $r = 1$, $f_n(r)$ can be then rewrite as

$$f_n(r) \sim \frac{A_n}{s_0^{1/4}} \left[e^{i(k_0 r + \gamma_n)} + e^{-i(k_0 r + \gamma_n + \pi/2)} \right]. \quad (16)$$

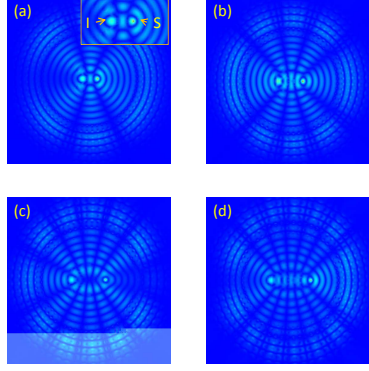


FIG. 4: Full-wave simulations of the design, with the excitation source placed at different locations. r_0 equals (a) 0.2, (b) 0.3, (c) 0.4, and (d) 0.5. The wavelength is fixed at 0.3, and the permittivity of metal is $\epsilon_m = -0.6 + 0.01i$. The amplitude of the magnetic field $|H|$ is plotted.

Coincidentally, a source at position \mathbf{r}_0 with $r_0 < 1$, *i.e.* inside the Eaton lens, generates a radiation such as

$$-\frac{i}{4}H_0^{(1)}(k_0|\mathbf{r}-\mathbf{r}_0|) = -\frac{i}{4}\sum_{-\infty}^{\infty}J_n(k_0r_<)H_n^{(1)}(k_0r_>)e^{in\phi}, \quad (17)$$

where $r_<$ is the smaller of r and r_0 , and $r_>$ is the larger of r and r_0 [20, 22]. The total magnetic field between r_0 and 1 is therefore given by

$$-\frac{i}{4}\sum_{-\infty}^{\infty}e^{in\phi}J_n(k_0r_0)\left[H_n^{(1)}(k_0r)+C_nH_n^{(2)}(k_0r)\right], \quad (18)$$

with C_n representing the amplitude of the reflected n -th order wave. When k_0 is large enough, the large argument approximations of the Hankel functions and the Bessel function lead to

$$J_n(k_0r_0)\left[H_n^{(1)}(k_0r)+C_nH_n^{(2)}(k_0r)\right] \approx \frac{2}{k_0\pi\sqrt{rr_0}}\cos(k_0r_0-\beta_n)\left[e^{i(k_0r-\beta_n)}+C_n e^{-i(k_0r-\beta_n)}\right], \quad (19)$$

with $\beta_n = (2n+1)\pi/4$. Again, we asymptotically match the above equation with $f_n(r)/\sqrt{r}$ of Equation (16), and finally achieve

$$C_n \sim e^{-i[(n+1)\pi+2\gamma_n]} = (-1)^{n+1}e^{-2i\gamma_n}, \quad A_n \sim \frac{2s_0^{1/4}}{k_0\pi\sqrt{r_0}}\cos(k_0r_0-\beta_n). \quad (20)$$

As mentioned at the beginning, an inside-out Eaton lens will convert light rays emitted from a source at position \mathbf{r}_0 , with $r_0 < 1$, to the opposite location $-\mathbf{r}_0$ and result in a perfect image. To extend this property to waves, it is required that

$$C_n = (-1)^{n+1}e^{-i\phi}, \quad (21)$$

with ϕ being the phase difference between the source and image. This relation can be easily obtained by time reversing the source radiation process [22]. Comparing Equation (21) with Equation (20), we obtain the following necessary condition for perfect imaging by an inside-out Eaton lens: *$e^{i2\gamma_n}$ must be constant and independent of the mode order n .* The function $e^{i2\gamma_n}$ can then be employed to partially evaluate the performance of a lens. For instance, we calculate the phase factor γ_n by using Equation (14), and the results are shown in Figure (2b). Evidently, γ_n are almost constant when λ is close to zero (the ray-optics region), while they vary strongly for a considerable wavelength.

In the following, we present a conceptual design consisting of a vacuum (background) and ideal metallic wires (a realistic device is currently under construction). First, the Maxwell-Garnett formula is used to approximate the effective permittivity of the composite (See Appendix B)

$$\epsilon_e = \frac{(1-f)+(1+f)\epsilon_m}{(1-f)\epsilon_m+(1+f)}, \quad (22)$$

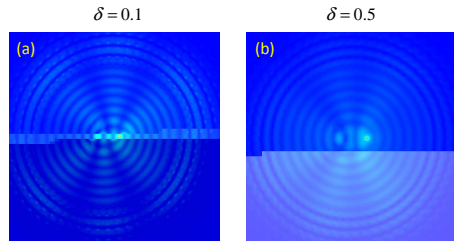


FIG. 5: The effect of metallic loss δ on the lens. The source is located at $r_0 = 0.2$. The wavelength λ is set to be 0.3 and $\text{Re}(\epsilon_m) = -0.6$.

with f being the filling fraction of the wires and ϵ_m being the permittivity of the ideal metal [22, 23]. Since ϵ_e should be equal to the permittivity of the Eaton lens, $(2 - r)/r$, the filling fraction is then given by

$$f(r) = (r - 1) \frac{1 + \epsilon_m}{1 - \epsilon_m}. \quad (23)$$

Notice that the first-order surface mode will be excited when $\epsilon_m = -1$ [23]. The designed lens, shown in Figure (3a), consists of 8 layers of metallic wires with different radii. The above equation is then used to determine the positions as well as the radii of these wires. The thickness of the p -th layer $a_{p+1} - a_p$ is set to be $a_p\pi/30$, with a_p and a_{p+1} being the inner and outer radius of the layer, respectively. Consequently we have

$$a_p = a_1(1 + \pi/30)^{p-1}, \quad (24)$$

where a_1 is assumed to be 0.95. Furthermore the following relation

$$(a_p - 1) \frac{1 + \epsilon_m}{1 - \epsilon_m} \approx \frac{\pi r_p^2}{a_p^2(\pi/30)^2}, \quad (25)$$

is employed to calculate the radius r_p of the wire in the p -th layer. In the current design, $\epsilon_m = -0.6 + i\delta$ with δ being very small, which leads to the wire radii shown in Figure (3b). Evidently, the wire radius increases rapidly with the increasing of r , with a minimum of 0.007 and a maximum of 0.06.

We employ a finite-element full-wave Maxwell solver to verify the above design [24], and plot the results with $\delta = 0.01$ in Figure (4). Notice that we always set $\lambda = 0.3$, a value much smaller than the lens size while big enough to ensure the validity of Equation (22). Clearly, an image is always observed at the location opposite to the source. To evaluate the quality of the image, we define

$$\eta = \left| \frac{H(-\mathbf{r}_0)}{H(\mathbf{r}_0)} \right|^2, \quad (26)$$

the ratio of the intensity of the image to that of the source. The bigger the η , the better the lens is. In Figure (4), the source location r_0 is gradually increased from 0.2 to 0.5, with an increment of 0.1. The corresponding η is found to be 0.21, 0.27, 0.15 and 0.15, respectively. Along the azimuthal direction, we observe a few intensity minima, and the total number of these minima depends on the source location r_0 . This phenomenon is very likely induced by the finite wavelength λ . One direct consequence is that different modes radiated from the source have quite different amplitudes, as given by $J_n(k_0 r_0)$ of Equation (17). For example, the zeroth-order and third-order modes dominate the radiation when $r_0 = 0.2$, while the ninth-order mode is the strongest one when $r_0 = 0.5$. We further investigate the influence of the metallic absorption in Figure (5), by setting $r_0 = 0.2$ and $\lambda = 0.3$. Two different δ , 0.1 and 0.5, are considered, and the corresponding intensity ratio η is found to be 0.11 and 0.06, respectively. Evidently, although the image quality is degraded with the increasing of the metallic absorption, the basic function of the Eaton lens, *i.e.* forming an image, still survives. We can partially interpret it with the fact that all the higher-order modes, such as $n > 25$, are totally reflected around $r = 1$. Only the low-order modes can propagate into the lens and hence be absorbed by the metal.

To summarize, we have studied two-dimensional inside-out Eaton lenses. The corresponding full wave equation is analytically solved with the help of the WKB approximation. One necessary condition for perfect imaging is further

found, *i.e.*, $e^{i2\gamma n}$ must be independent of the mode order n . Furthermore, a general design procedure of the lens, based on effective medium theory, is developed. We present one example consisting of metal wires with different radii, and further verify the design with a full wave Maxwell solver. Its dependence on source location as well as metallic absorption is also investigated.

This work was supported in part by the Penn State MRSEC under NSF grant no. DMR 0213623.

Appendix A: A ray-optics theory of the Eaton lens

A detailed description regarding the ray-optics theory of the Eaton lens can be found in Reference [6]. We briefly repeat it here for the reader's convenience.

In geometric optics, there are two different but equivalent ways to describe the trajectory of a light ray. The first one is the Newtonian Euler-Lagrange equation

$$\frac{d^2\mathbf{r}}{d\xi^2} = \frac{\nabla n^2(\mathbf{r})}{2}, \quad (\text{A.1})$$

where n is the refractive index and the parameter ξ is given by $d\xi = dr/n$. We can interpret the above equation by using Newton's law, $m\mathbf{a} = -\nabla U$, for a mechanical particle with unit mass moving in "time" ξ under the influence of potential $U = -n^2/2 + E$, with E being an arbitrary constant. The second way is based on Hamilton's equation

$$\frac{d\mathbf{r}}{dt} = \frac{c}{n} \frac{\mathbf{k}}{k}, \quad \frac{d\mathbf{k}}{dt} = \frac{ck}{n^2} \nabla n(\mathbf{r}), \quad (\text{A.2})$$

with \mathbf{k} being the wave vector and c being the speed of light in free space. Notice that by treating frequency $\omega = ck/n$ as the Hamiltonian, the above equation resembles the standard form of Hamilton's equation.

We can define an angular momentum as

$$\mathbf{L} = \mathbf{r} \times \frac{d\mathbf{r}}{d\xi} = \frac{n}{k} \mathbf{r} \times \mathbf{k}, \quad (\text{A.3})$$

which leads to

$$\frac{d\mathbf{L}}{d\xi} = \mathbf{r} \times \frac{d^2\mathbf{r}}{d^2\xi} = \frac{1}{2} \mathbf{r} \times \nabla n^2 = \frac{dn^2}{dr} \frac{\mathbf{r} \times \mathbf{r}}{2r} = 0, \quad (\text{A.4})$$

when the refractive-index profile $n(r)$ is spherically symmetric. The above equation suggests that the angular momentum \mathbf{L} is conserved. Hence, a family of light rays propagating in the xy plane at the beginning will always stay in the same plane. This fact implies that a two-dimensional Eaton lens with similar refractive-index profile $n(r)$ functions identically to the three-dimensional one.

To solve the two-dimensional Newtonian Euler-Lagrange equation, it is convenient to introduce the complex number $z = x + iy$, and further reformulate the equation as

$$\frac{d^2 z}{d\xi^2} = \frac{z}{2r} \frac{dn^2}{dr} = -\frac{1}{r^3} z = -\frac{1}{|z|^3} z, \quad (\text{A.5})$$

by substituting the refractive index of the Eaton lens $n(r) = \sqrt{(2-r)/r}$. The solution, following Equation (6.13) and (6.14) of Reference [6], can be expressed as

$$z = e^{i\alpha} [\cos(2\xi') + i \sin \gamma \sin(2\xi') + \cos \gamma], \quad d\xi = 2|z|d\xi', \quad (\text{A.6})$$

which describes displaced ellipses rotated by the angle α .

Appendix B: Maxwell-Garnett Formula

Consider a two-component mixture composed of inclusions embedded in an otherwise homogeneous matrix, where ϵ_m and ϵ_d are their respective dielectric functions. The average electric field $\langle \mathbf{E} \rangle$ over one unit area surrounding the point \mathbf{x} is defined as

$$\langle \mathbf{E}(\mathbf{x}) \rangle = \frac{1}{A} \int_A \mathbf{E}(\mathbf{x}') d\mathbf{x}' = f \langle \mathbf{E}_m(\mathbf{x}) \rangle + (1-f) \langle \mathbf{E}_d(\mathbf{x}) \rangle, \quad (\text{B.1})$$

with f being the volume fraction of inclusion. A similar expression can be obtained for the average polarization

$$\langle \mathbf{P}(\mathbf{x}) \rangle = f \langle \mathbf{P}_m(\mathbf{x}) \rangle + (1 - f) \langle \mathbf{P}_d(\mathbf{x}) \rangle. \quad (\text{B.2})$$

We further assume that the following constitutive relations are valid

$$\langle \mathbf{P}_m(\mathbf{x}) \rangle = \epsilon_0(\epsilon_m - 1) \langle \mathbf{E}_m(\mathbf{x}) \rangle, \quad \langle \mathbf{P}_d(\mathbf{x}) \rangle = \epsilon_0(\epsilon_d - 1) \langle \mathbf{E}_d(\mathbf{x}) \rangle, \quad (\text{B.3})$$

and the average permittivity tensor of the composite medium is defined by

$$\langle \mathbf{P}(\mathbf{x}) \rangle = \epsilon_0(\bar{\epsilon}_e - \bar{\mathbf{I}}) \cdot \langle \mathbf{E}(\mathbf{x}) \rangle. \quad (\text{B.4})$$

Combining the above equations we can obtain the effective permittivity $\bar{\epsilon}_e$. Clearly the resultant $\bar{\epsilon}_e$ depends on the relationship between $\langle \mathbf{E}_m(\mathbf{x}) \rangle$ and $\langle \mathbf{E}_d(\mathbf{x}) \rangle$ [25].

We now assume that the inclusion has the shape of a cylinder, and its radius is far smaller than the wavelength so that its optical properties can be well described by the electrostatic equation

$$\nabla \cdot (\epsilon(\mathbf{r})\phi) = 0. \quad (\text{B.5})$$

By matching the boundary conditions we can prove that $\phi_m/\phi_0 = 2\epsilon_d/(\epsilon_d + \epsilon_m)$, where ϕ_m is the total potential inside the cylinder when the external electric field $-\nabla\phi_0$ is homogeneous. This relation is further used to obtain the electric field [26]. It is finally found that the average permittivity is scalar and can be expressed as

$$\epsilon_e = \epsilon_d \frac{(1 - f)\epsilon_d + (1 + f)\epsilon_m}{(1 - f)\epsilon_m + (1 + f)\epsilon_d}, \quad (\text{B.6})$$

consistent with the Maxwell-Garnett dielectric function. Equivalently we can express the filling fraction as

$$f(r) = \frac{(\epsilon_e - \epsilon_d)(\epsilon_m + \epsilon_d)}{(\epsilon_e + \epsilon_d)(\epsilon_m - \epsilon_d)}. \quad (\text{B.7})$$

-
- [1] C. Gomez-Reino, M. V. Perez, and C. Bao, *Gradient-Index Optics: Fundamentals and Applications* (Springer, 2002).
[2] J. C. Maxwell, "Solutions of Problems," *Camb. Dublin Math. J.* 8, 188 (1854).
[3] R. K. Luneburg, *Mathematical Theory of Optics* (University of California Press, 1964).
[4] J. E. Eaton, "On Spherically Symmetric Lenses," *Trans. IRE Antennas Propag.* 4, 66 (1952).
[5] U. Leonhardt and T. G. Philbin, "Transformation Optics and the Geometry of Light," *Prog. Opt.* 53, 69 (2009).
[6] U. Leonhardt and T. G. Philbin, *Geometry and Light: The Science of Invisibility* (Dover Publications, 2010).
[7] Y. G. Ma, C. K. Ong, T. Tyc, and U. Leonhardt, "An Omnidirectional Retroreflector Based on the Transmutation of Dielectric Singularities," *Nat. Materials* 8, 639 (2009).
[8] N. Kundtz and D. R. Smith, "Extreme-angle Broadband Metamaterial Lens," *Nat. Materials* 9, 129 (2010).
[9] V. N. Smolyaninova, I. I. Smolyaninov, A. V. Kildishev, and V. M. Shalaev, "Maxwell Fish-eye and Eaton Lenses Emulated by Microdroplets," *Opt. Lett.* 35, 3396 (2010).
[10] D. R. Smith, Y. Urzhumov, N. B. Kundtz, and N. I. Landy, "Enhancing Imaging Systems Using Transformation Optics," *Opt. Express* 18, 21238 (2010).
[11] T. Zentgraf, Y. Liu, M. H. Mikkelsen, J. Valentine, and X. Zhang, "Plasmonic Luneburg and Eaton lenses," *Nat. Nanotechnology* 6, 151 (2011).
[12] U. Leonhardt, "Perfect Imaging Without Negative Refraction," *New J. Phys.* 11, 093040 (2009).
[13] J. B. Pendry, "Negative Refraction Makes a Perfect Lens," *Phys. Rev. Lett.* 85, 3966 (2000).
[14] L. Solymar and E. Shamonina, *Waves in Metamaterials* (Oxford University, 2009).
[15] J. B. Pendry, D. Schurig, and D. R. Smith, "Controlling Electromagnetic Fields," *Science* 312, 1780 (2006).
[16] U. Leonhardt, "Optical Conformal Mapping," *Science* 312, 1777 (2006).
[17] D.-H. Kwon and D. H. Werner, "Transformation Electromagnetics: An Overview of the Theory and its Application," *IEEE Antennas Prop. Mag.* 52, 24 (2010).
[18] H. Chen, C. T. Chan, and P. Sheng, "Transformation Optics and Metamaterials," *Nat. Materials* 9, 387 (2010).
[19] D. R. Smith, W. J. Padilla, D. C. Vier, S. C. Nemat-Nasser, and S. Schultz, "Composite Medium with Simultaneously Negative Permeability and Permittivity," *Phys. Rev. Lett.* 84, 4184 (2000).
[20] W. C. Chew, *Waves and Fields in Inhomogeneous Media* (IEEE Press, 1995).
[21] J. J. Sakurai, *Modern Quantum Mechanics* (Revised Ed. Addison-Wesley, 1994).
[22] J. D. Jackson, *Classical Electrodynamics* (3rd Edition, John Wiley & Sons, 2004).

- [23] Y. Zeng, Q. Wu and D. H. Werner, "Electrostatic Theory for Designing Lossless Negative Permittivity Metamaterials," *Opt. Lett.* 35, 1431 (2010).
- [24] COMSOL, www.comsol.com.
- [25] C. F. Bohren and D. R. Huffman, *Absorption and Scattering of Light by Small Particles* (John Wiley & Sons, 1998).
- [26] Y. Zeng, J. Liu and D. H. Werner, "General Properties of Two-dimensional Conformal Transformations in Electrostatics," Submitted for publication.